SAND79-2126
Unlimited Release

UC-25

A Consistent Stress-Strain Ductile Fracture Model as Applied to Two Grades of Beryllium

Tom G. Priddy, Steve E. Benzley, L. Mike Ford

2900 Q(7-73)

SAND79-2126
Unlimited Release

A CONSISTENT STRESS-STRAIN DUCTILE FRACTURE MODEL AS APPLIED TO TWO GRADES OF BERYLLIUM*

T. G. Priddy, S. E. Benzley, and L. M. Ford
Applied Mechanics Division 5522
Sandia Laboratories†
Albuquerque, New Mexico 87185

ABSTRACT

Published yield and ultimate biaxial stress and strain data for two grades of beryllium are correlated with a more complete method of characterizing macroscopic strain at fracture initiation in ductile materials. Results are compared with those obtained from an exponential, mean stress dependent, model. Simple statistical methods are employed to illustrate the degree of correlation for each method with the experimental data.

---

* This work was supported by the U. S. Department of Energy under Contract AT(29-1)-789.

† A U. S. Department of Energy Facility.

A Consistent Stress-Strain Ductile Fracture Model as Applied to Two Grades of Beryllium

INTRODUCTION

Two methods of correlating effective plastic strain at fracture of ductile solids are discussed in this report. One of these is a mathematical model based upon void growth kinematics noted by McClintock[1] and by Rice and Tracey[2]. These results provide evidence of rapidly decreasing ductility with the tensile mean stress. Hancock and MacKenzie[3] used Rice and Tracey's results to represent the effective plastic strain at fracture as

$$\bar{\varepsilon}_p = A \exp^{-\frac{3}{2}\left(\sigma_m/\bar{\sigma}\right)} \qquad (1)$$

where the ductility as measured in terms of the effective plastic strain (i.e., square root of the second invariant of the deviator strain tensor) at fracture is a function of the average stress σ_m, and $\bar{\sigma}$ which is the root mean square of the "principal shear stresses". This equation was used to good advantage by Hancock and MacKenzie in the correlation of experimental data taken from tests of various high strength steels.

---

[1]Superscript numbers refer to similarly numbered references at end of report.

The second method of analysis is an extension of the dual strength characterization model reported in Reference (4). In this previous study a mathematical model of fracture in multi-axial stress space was proposed. Yield and ultimate strength surfaces for two grades of beryllium were jointly displayed. These surfaces were quantified and compared with experimental data reported by Lindholm, et al.[5] Ductility (the stress-space region which corresponds to plastic flow) was shown to decrease under triaxial stress and vanish at the intersection of the yield and ultimate surfaces. While this stress space model is theoretically complete for work hardening materials, plastic strain at fracture is a more convenient, sensitive, and practical measure of ductility. Also, because the strain data scatter may be wider than the associated scatter in the strength data, statistical bounds based on strain measurements are desired.

The data for the two grades of beryllium measured by Lindholm et al[5] have therefore been re-studied to:

1. correlate the beryllium failure strain data with a mathematical model,

2. introduce a failure stress to failure strain transformation model to be used in conjunction with the stress space model of Reference 4, and

3. show that the three elements: stress at fracture, strain at fracture, and a failure stress to failure strain model can be jointly used to consistently characterize macroscopic fracture of ductile solids.

Data reduction and correlation using Equation (1), were also attempted and these results are illustrated for comparison with those from the current model. Elementary statistical methods were used to predict data scatter bounds and to indicate the precision of the separate methods.

DISCUSSION OF MATHEMATICAL MODELS

Two methods are used in this study to correlate the strain data measured by Lindholm, et al. for two grades of beryllium. The exponential model, Equation (1) was generalized by substituting an unknown but to be determined constant (k) for the factor 3/2, i.e.,

$$\bar{\varepsilon}_p = A \exp -k\left(\sigma_m/\bar{\sigma}\right) \qquad (2)$$

The parameters in Equation (2) are defined for use in this study by Equations (3):

$$\bar{\varepsilon}_p = \frac{\sqrt{2}}{3}\left[(\varepsilon_1-\varepsilon_2)^2 + (\varepsilon_2-\sigma_3)^2 + (\varepsilon_3-\varepsilon_1)^2 + 6\left(\varepsilon_{12}^2 + \varepsilon_{23}^2 + \varepsilon_{31}^2\right)\right]^{1/2}$$

$$\sigma_m = \frac{1}{3}\left(\sigma_1 + \sigma_2 + \sigma_3\right) \qquad (3)$$

$$\bar{\sigma} = \frac{1}{\sqrt{2}}\left[(\sigma_1-\sigma_2)^2 + (\sigma_2-\sigma_3)^2 + (\sigma_3-\sigma_1)^2 + 6\left(\tau_{12}^2 + \tau_{23}^2 + \tau_{31}^2\right)\right]^{1/2}$$

where;

A = constant to be determined from test data and

k = constant, determined simultaneously with the parameter A from two independent states of stress-strain data at fracture.

This exponential model is described well in the referenced literature and it is founded on experimental observation and calculations ot the kinematics ot void growth. The model is expected to be limited to a particular range of tensile mean stress, however, since pure dilatation should lead to fracture without plastic strain and the model predicts a rapid increase in ultimate plastic strain (and strength) with compressive mean stress.

The second method of analysis is an extension of the dual strength characterization model reported in Reference (4). In that report, a wide range of biaxial strength data were accurately correlated with the cubic stress space model given in Reference (6). Figure (1) is an illustration of this dual yield and ultimate strength model. Note that in the deviatoric plane the ultimate surface is not circular. A scalar function of stress such as $\bar{\sigma}$ is not constant on this surface at a fixed value of σ_m but has rotational dependence. The parameter τ is used to make this distinction. τ is defined as the amplitude of the deviatoric stress vector and it is calculated from a principal stress state with Equation (4).

$$\tau = \frac{1}{\sqrt{3}} \left[(\sigma_1-\sigma_2)^2 + (\sigma_2-\sigma_3)^2 + (\sigma_3-\sigma_1)^2 \right]^{1/2} \qquad (4)$$

The use of the parameter τ provides a true perspective in a geometrical sense for the stress space surfaces and its magnitude at a point on each surface is a function of the various combinations of deviatoric stress components as well as the mean stress. Figure (2) shows how the direction and magnitude of the deviatoric stress vector would be oriented for the failure conditions under pure shear, uniaxial tension, and equal biaxial tension states of stress.

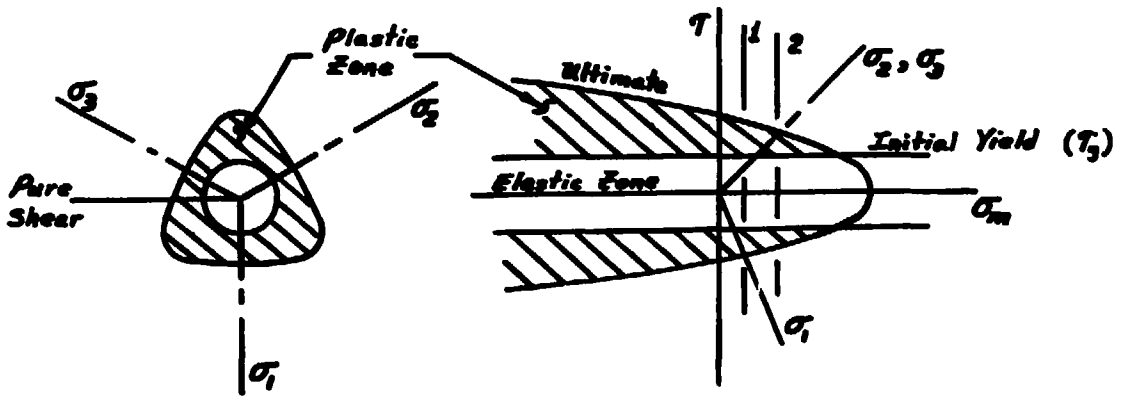

Figure 1
Dual Characterization Stress Space Model

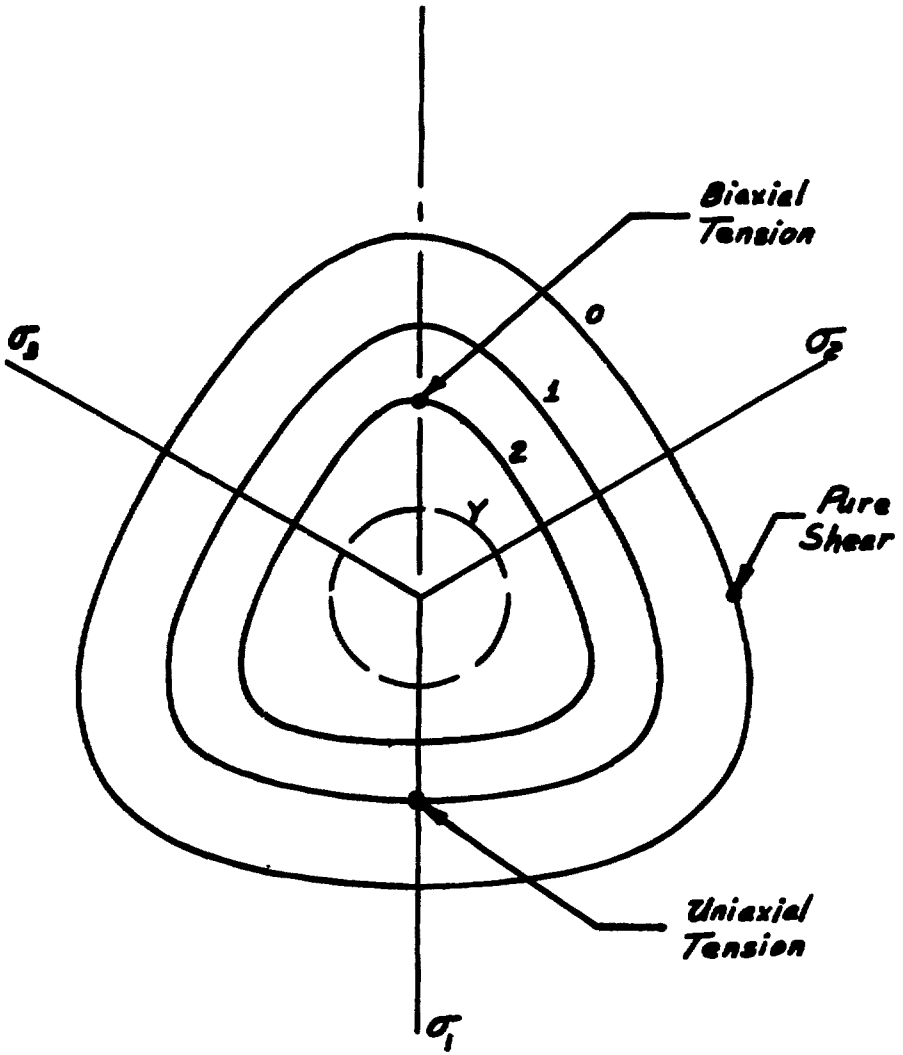

Figure 2
Deviatoric Strength Contours for Various Deviatoric Planes

Extension of this stress-space model to predict strain at fracture requires a failure stress to failure strain transformation model. A stress-strain model is also required in the stress analysis but the needs are different. In the stress analysis the entire path of a stress-strain curve must be accurately traced while correlation of ultimate strain to ultimate stress needs to only model the terminal points on such a curve. A truncated power series, Equation (5), is proposed to correlate these terminal point data. A general stress-strain curve is illustrated in Figure (3) as an aid in graphical interpretation of terms in this equation.

$$\bar{\varepsilon}_p = a + b\left(\frac{\tau_u - \tau_y}{\tau_y}\right) + c\left(\frac{\tau_u - \tau_y}{\tau_y}\right)^2 + \ldots \qquad (5)$$

(Recall that $\tau_u = \tau_u(\sigma_m, \text{ loading path})$.) Plastic strain is assumed to be measured by $\bar{\varepsilon}_p$ and is assumed to be totally driven by the deviatoric (flow) stress. In the general curve, an unstable plastic strain increment can be equated to the constant term in the series of Equation (5). A varying slope of the stress strain curve in the terminal region can be accommodated by the second and third terms. For materials which do not exhibit an unstable flow region, as depicted in Figure (4), the constant term, a, would be zero. This latter condition is assumed appropriate for analysis of the beryllium data. The other constants, b and c, remain to be quantified in this case and strain data which correspond to two independent

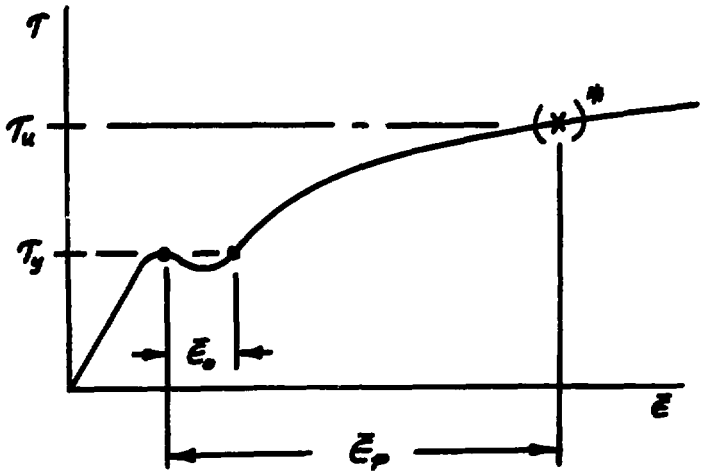

Figure 3
General Stress - Strain Curve

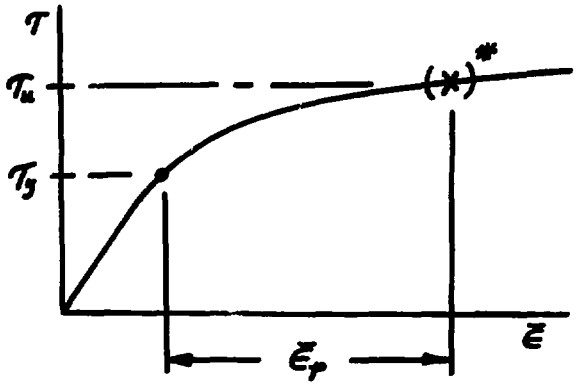

Figure 4
Stable Stress - Strain Curve for
Work Hardening Materials

---

* Note that τ_u and $\bar{\varepsilon}_p$ are variables which depend upon σ_m and the loading path to fracture. The points (X) located on these curves are shown for illustration purposes.

stress conditions necessary to quantify the stress space model were used to calculate values for these constants.

The ultimate deviatoric stress level, τ_u, can be calculated from the cubic model of Ref. (4). The magnitude of deviatoric stress at initial yield is denoted by τ_y. The corresponding plastic strain at fracture can then be calculated with Equation (5). Equation (5) offers a simple form for treating both unstable flow and a hardening rule where hardening either increases or decreases with increased plastic strain. As shown later in this report this simple equation quite accurately correlates the beryllium strength and ultimate strain data.

In summary, two independent states of stress with corresponding measurements of effective plastic strain are required to define the constants in these equations. For the two grades of beryllium, uniaxial tension and pure shear data were selected. The remaining data points were used to test the ability of the mathematical models to predict the measured plastic strain at fracture.

DATA ANALYSIS

The following steps were taken in analyzing the strain and stress at fracture for the two grades of beryllium reported in Reference (5):

1. The ultimate and yield strengths were previously correlated with the dual characterization methods presented in Reference (4). Only those curves used in the correlation of strain data are repeated in this report. These are Figures (5 and 6) which are plots of deviatoric vs. mean stress strength curves for the Be-XN50C and Be-P1 data. The bounds were determined from calculations of plus and minus two standard deviations on the input data. Uniaxial tension and pure shear were used for these ultimate strength input data. Other curves in Reference (4) show that these methods provided accurate bounds for the biaxial strength data.

2. The complete data sets were separated into three subsets: uniaxial tension, pure shear, and the remaining stress conditions (called the "remainder"). The ultimate data were reduced to $\bar{\varepsilon}_f$, τ_u, and σ_m. To calculate $\bar{\varepsilon}_p$ from only two measured components of strain, incompressibility, as given by Equation (6), was assumed and used to calculate the third component of strain,

$$\varepsilon_1 + \varepsilon_2 + \varepsilon_3 = 0 \qquad (6)$$

where ε_1 and ε_2 are the two principal strain components reported in Reference (5).

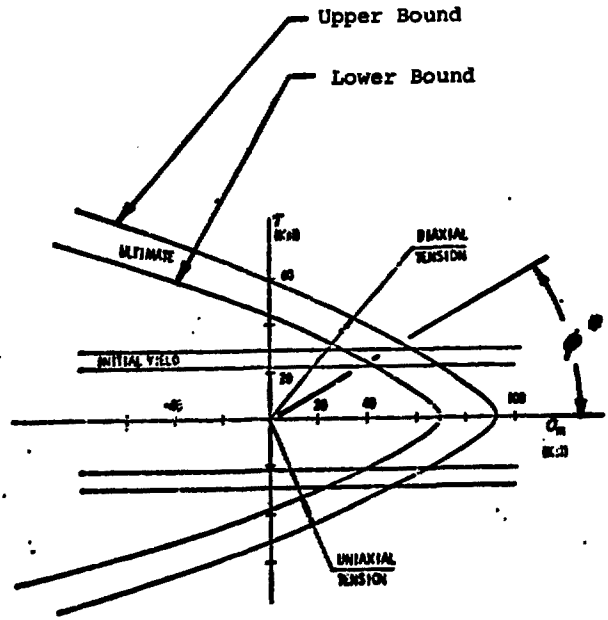

Figure 5

Plot of Deviatoric
vs. Mean Stress Strengths
for Be-XN-50C

---

* Note that $\sigma_m/\tau = \cot(\phi)$. Data are plotted versus this ratio (σ_m/τ) in several figures later in this report. This ratio is used since it provides a convenient parameter for spanning the various stress states in (τ, σ_m) stress space.

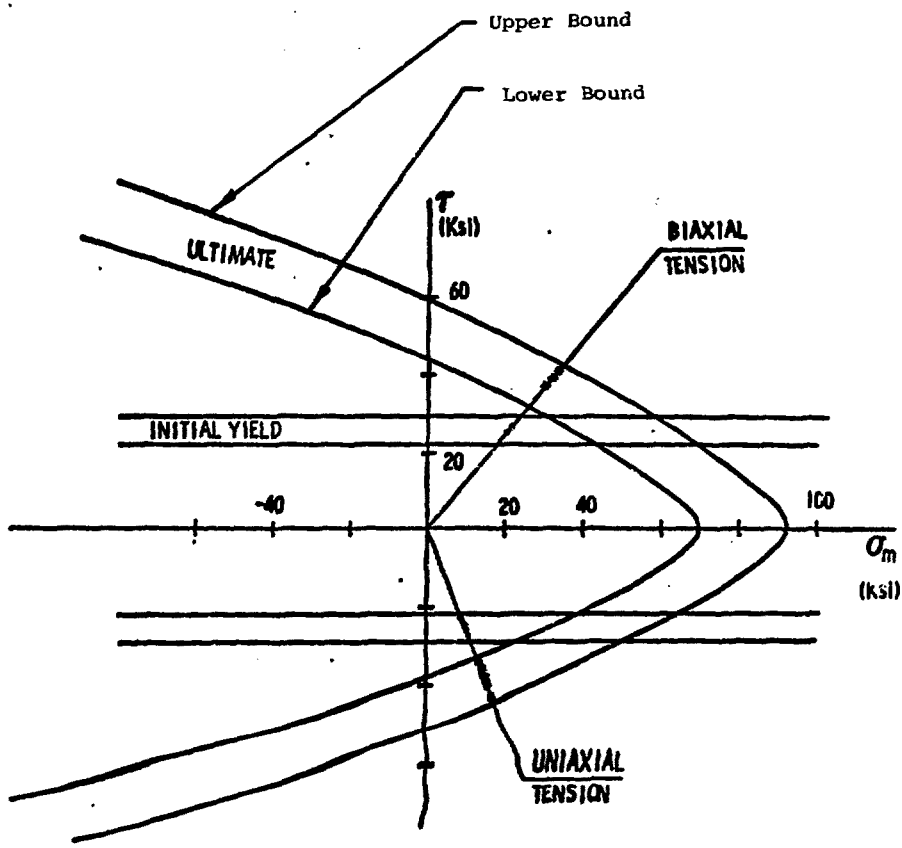

Figure 6

Plot of Deviatoric vs. Mean Stress Strengths for Be-Pl.

Additionally, the strain measurements reported in Reference (5) were total components of strain; i.e., they included the strain to 0.2% offset yield. The effective plastic strain was computed by subtracting a constant value of strain at 0.2% offset yield from the total effective strain determined with the first of Equations (3) and the referenced measurements.

Some of the test specimens had been pre-strained but in this analysis, these various stress paths to fracture were not considered. Deviatoric stress, τ_u, and mean stress, σ_m, at fracture were computed for each data point with the forms given in Equations (4 and 3) respectively. The deviatoric yield strength, τ_y, was taken as the average tensile yield strength calculated in Reference (4): $\tau_y = 30.5$ Ksi for Be-XN50C and $\tau_y = 41.3$ Ksi for Be-P1.

3. Constant (a) in Equation (5) was set to zero and constants (b and c) were determined from the uniaxial tension and pure shear data. Average values of the reduced data, τ_u and $\bar{\varepsilon}_p$, were calculated for the separate input data sets; uniaxial tension and pure shear. These two sets of average values were inserted into Equation (5) to form two simultaneous algebraic equations. These were solved for the constants (b and c).

4. Equation (5) was normalized by dividing both sides of this equation with the right hand side to develop a function of both stress and strain which should provide a dimensionless quantity for each data point. These data should be centered about unity if the correlation scheme is useful; i.e.,

$$F = \frac{\bar{\varepsilon}_p}{b\left(\frac{\tau_u - \tau_y}{\tau_y}\right) + c\left(\frac{\tau_u - \tau_y}{\tau_y}\right)^2} \qquad (7)$$

note that F is unity when average values of $\bar{\varepsilon}_p$ and τ_u from the input data sets are inserted into Equation (7). Standard deviation of F was calculated for the completed set of input data. Calculated values of b, c, and the standard deviation of F are given in Table (I) for the two sets of measured data. Figures (7 and 8) are scatter plots of these reduced input data vs. σ_m/τ for the two materials. Plus and minus two standard deviation values of F are shown with the vertical lines. Figures (9 and 10) show the scatter in the reduced values of plastic strain vs σ_m/τ.

5. To test the applicability of Equation (7), values of F were computed for the additional data. Figures (11 and 12)

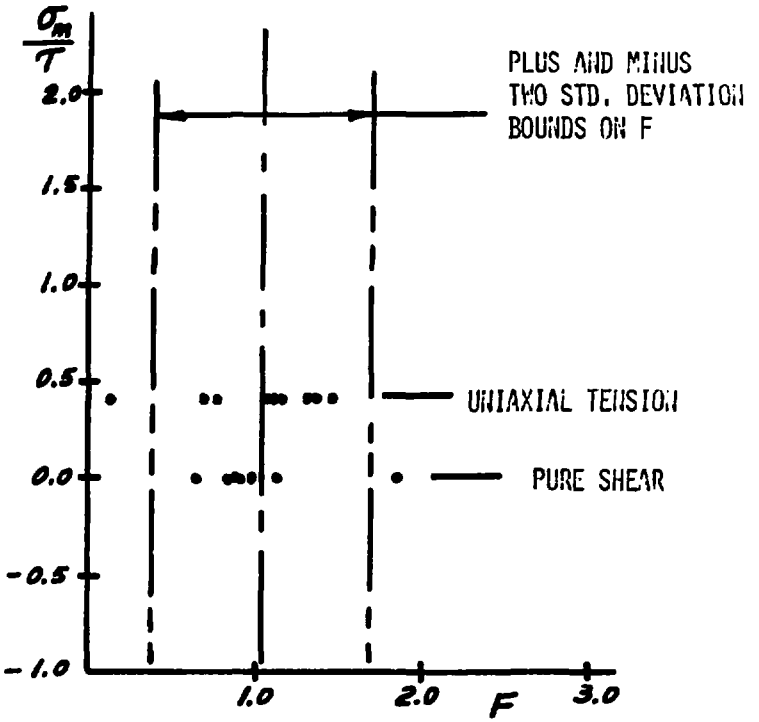

Figure 7
Plot of Reduced Be-XN50C Input Data

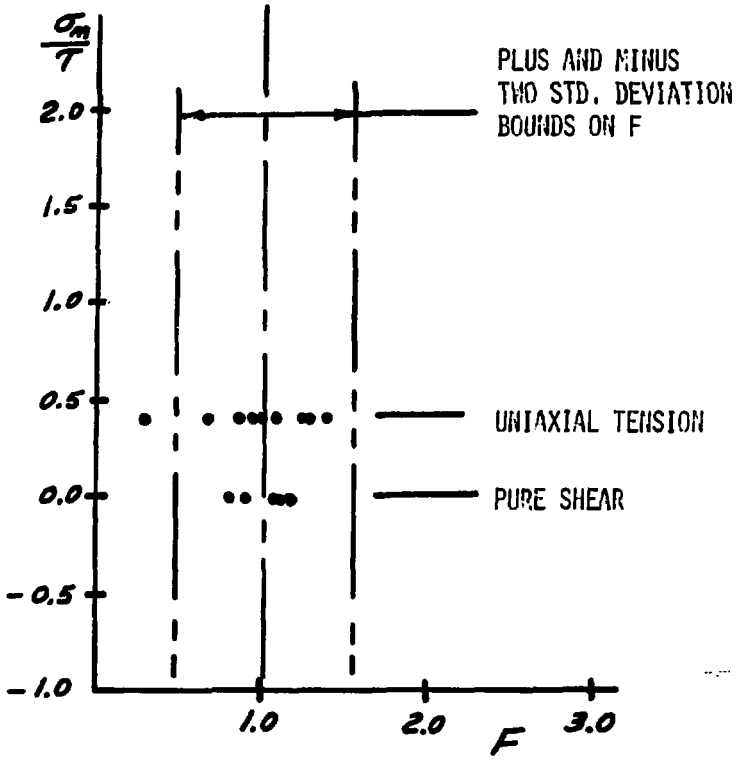

Figure 8
Plot of Reduced Be-Pl Input Data

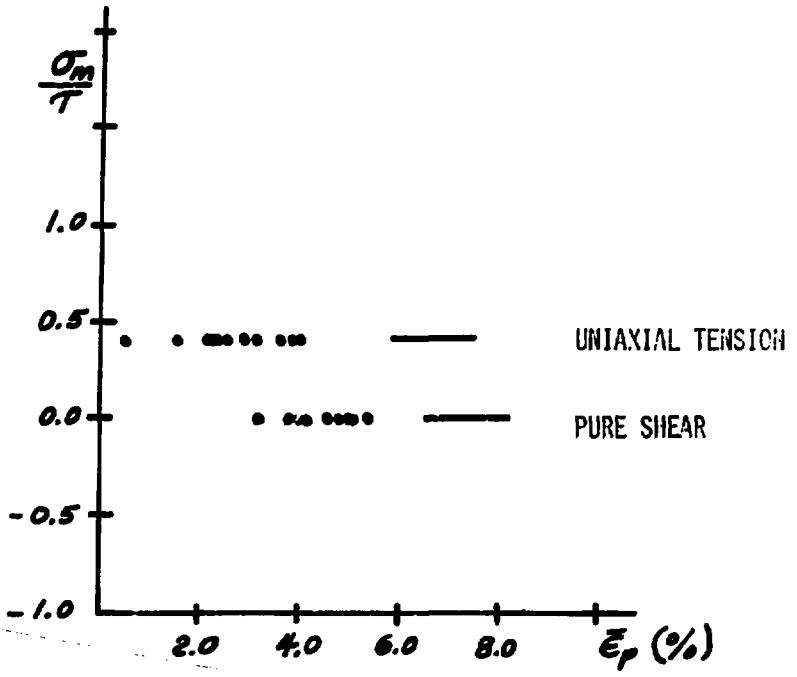

Figure 9
Plot of Be-XN50C Effective Plastic Strain vs. σ_m/T, Input Data

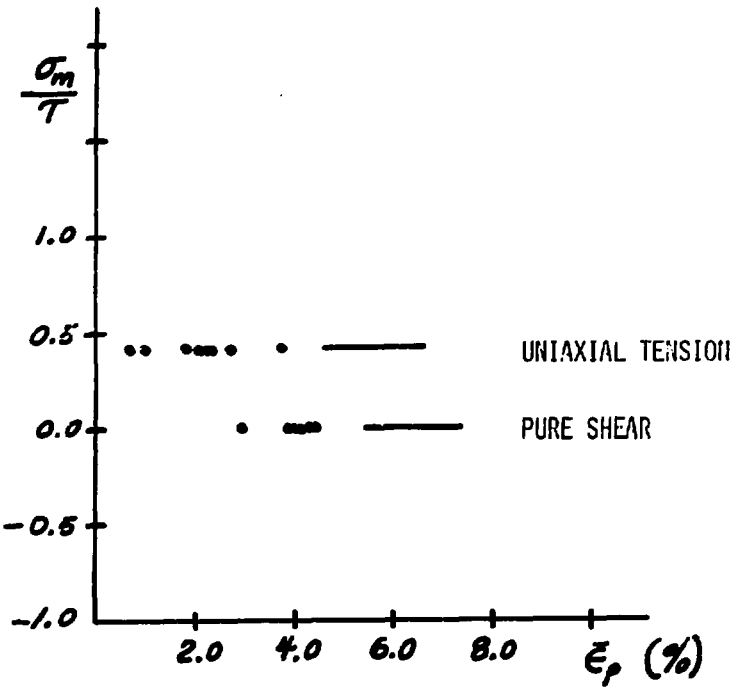

Figure 10

Plot of Be-Pl Effective Plastic Strain vs. $\sigma_m/\bar{\tau}$, Input Data

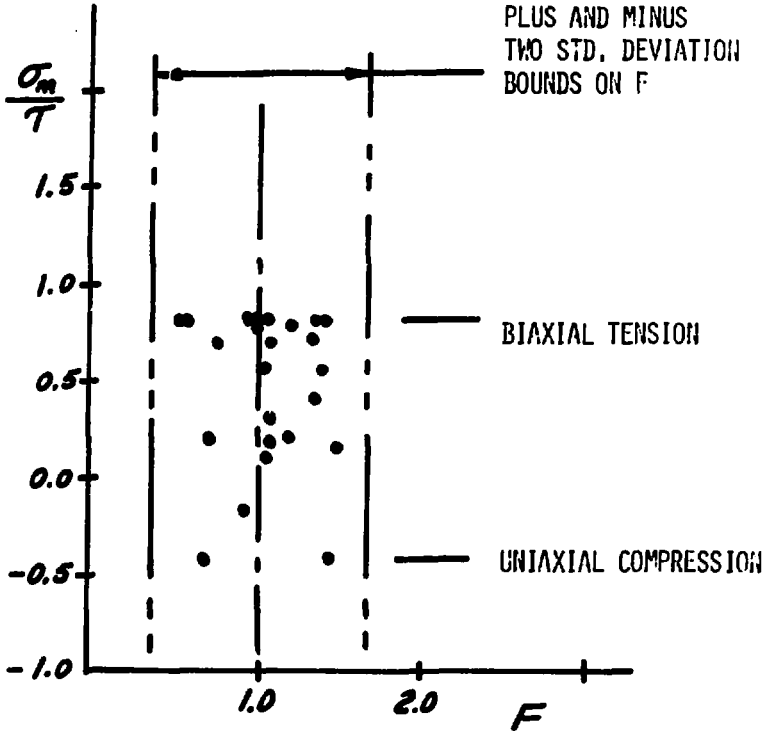

Figure 11
Plot of Reduced Be-XN50C Data,
Remainder Data Set

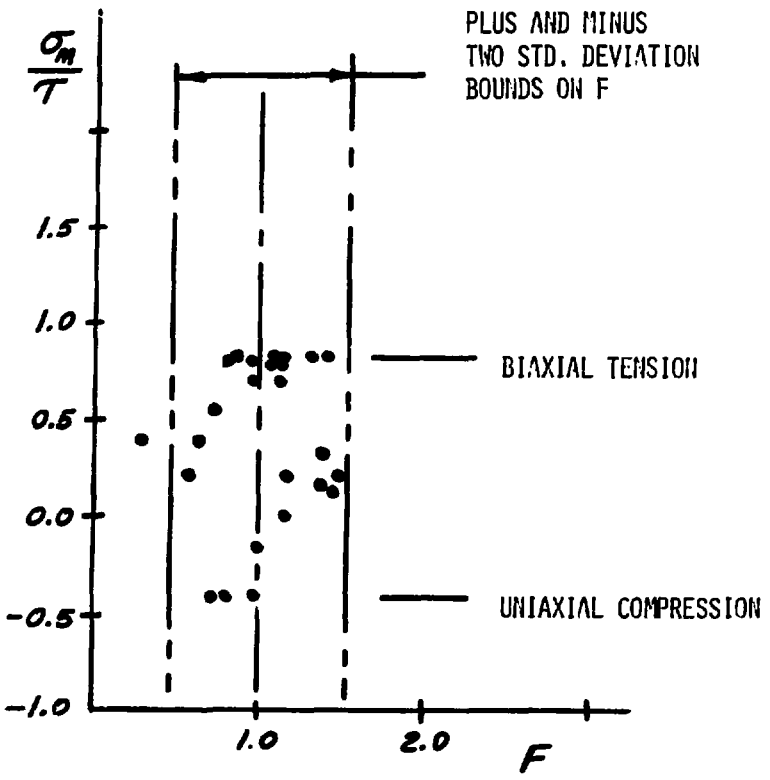

Figure 12
Plot of Reduced Be-Pl Data,
Remainder Data Set

are plots of F vs. σ_m/τ for these data. The bounds are those previously calculated from the selected input data. Note that these data are essentially contained and centered within the bounds. Histograms of these data were constructed to further test the assumption made in applying Equation (7) through Figures (7, 8, 11 and 12) that the complete set of data is normally distributed about the mean value of unity. Figure (13) is a histogram plot for the Be-XN50C data set. Similar results were obtained for the Be-P1 data and are shown in Figure (14).

TABLE I

Calculated Constants for Two Grades of Be for Use in Eq (5)

	b	c	Std. Deviation of F for Input Data	Number of Input Data Points
XN50C	4.442	0.20	0.326	23
P1	3.079	1.792	0.265	17

6 To test the transformation from stress space to effective plastic strain, the outer and inner ultimate strength bounds from Figures (5 and 6) were transformed with Equation (5) and these are displayed in Figures (15 and 16). The stress vector orientation was preserved in these plots. The biaxial tension and uniaxial tension data points are also plotted. Note that the measured biaxial

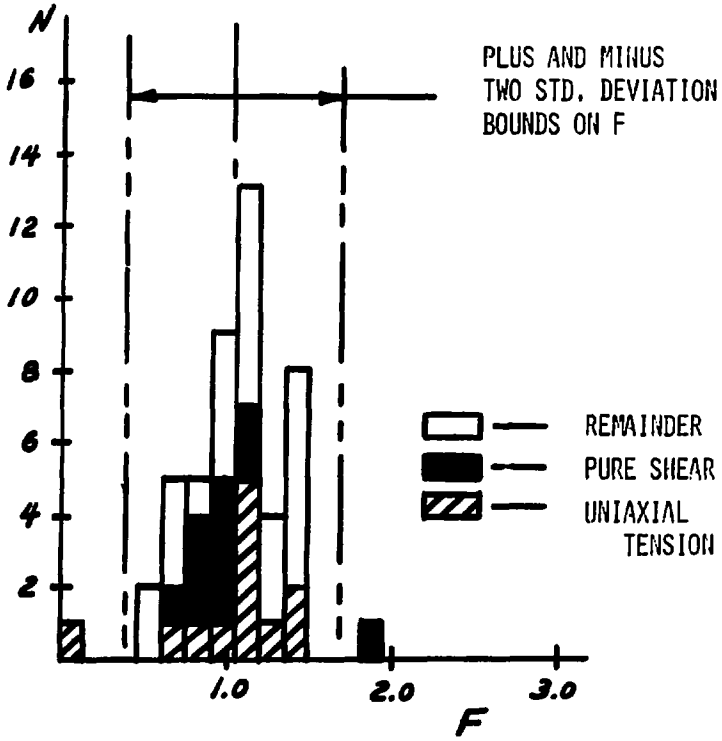

Figure 13
Histogram Plot of Reduced Be-XN50C Data

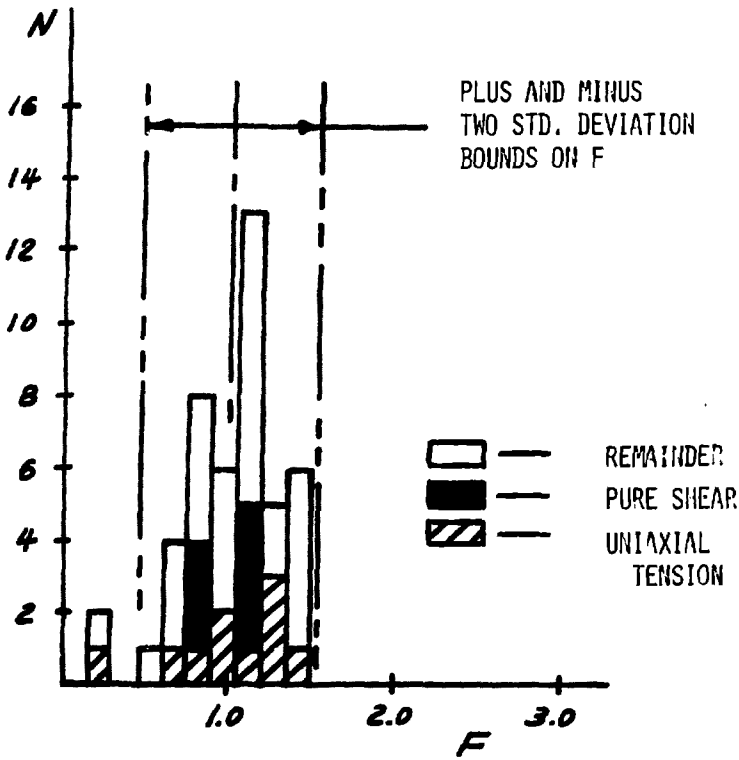

Figure 14
Histogram Plot of Reduced Be-Pl Data

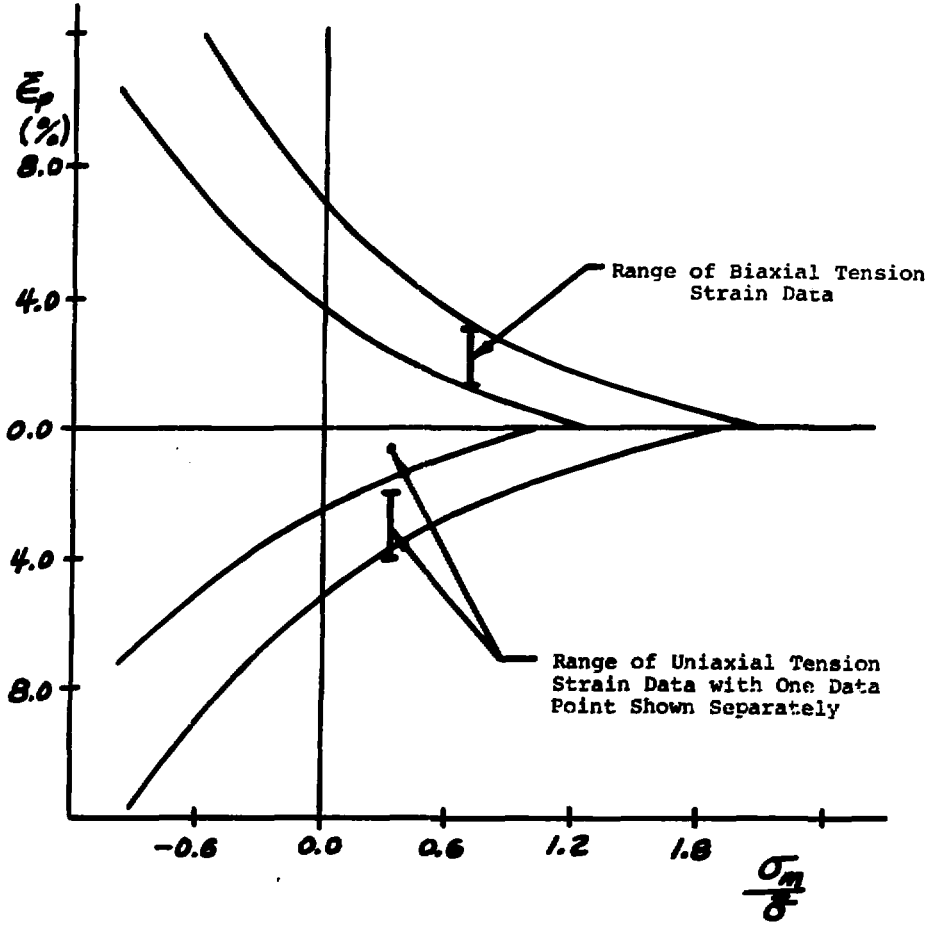

Figure 15

Transformed Stress Space Bounds, Be-XN50C, Plotted vs. $\sigma_m/\bar{\sigma}$

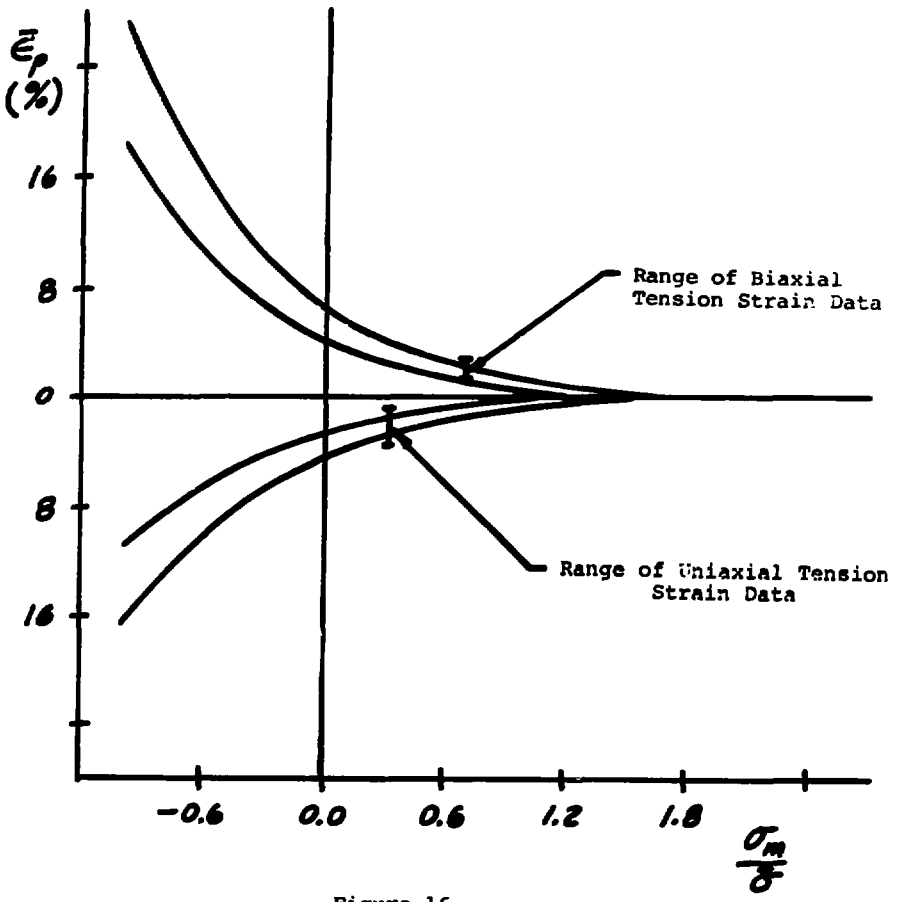

Figure 16
Transformed Stress Space Bounds, Be-Pl,
Plotted vs. $\sigma_m/\bar{\sigma}$

tension strain data are compared with bounding curves which are developed totally from the stress-space model, uniaxial tension and pure shear strengths, calculated variations in these input strength measurements, and the failure strain to failure stress rule given by Equation (5). The uniaxial tension data were used as part of the input data to the modeling equations but the stress-space orientation of these data relative to the biaxial tension data should be noted. This rotational significance, illustrated in Figure (2), is attributed to the third stress invariant which was included in the stress space model.

Another method of illustrating transformed strain at fracture is displayed in Figures (17 and 18). The deviatoric stress along the average ultimate surface was transformed to strain using Equation (5) and was plotted versus mean stress normalized with the average ultimate tensile strength. Plus and minus two standard deviation strain scatter bounds were computed from the uniaxial tension and pure shear data and these were added to and subtracted from the calculated average values to form the displayed scatter bounds. The reduced biaxial tension data are plotted to illustrate how well they are contained with these predictive methods. It is interesting to note that the effective plastic strain at failure is essentially a linear function of mean stress at failure for these grades of beryllium.

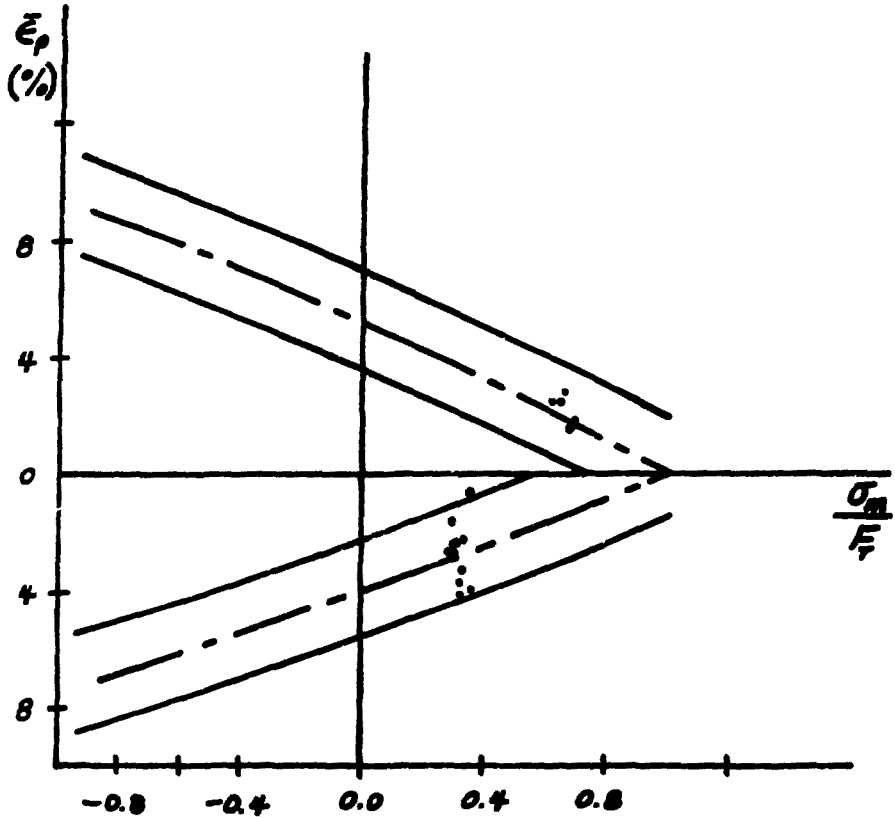

Figure 17

Transformed Stress Space Bounds,
Be-XN50C, Plotted vs. σ_m/F_T

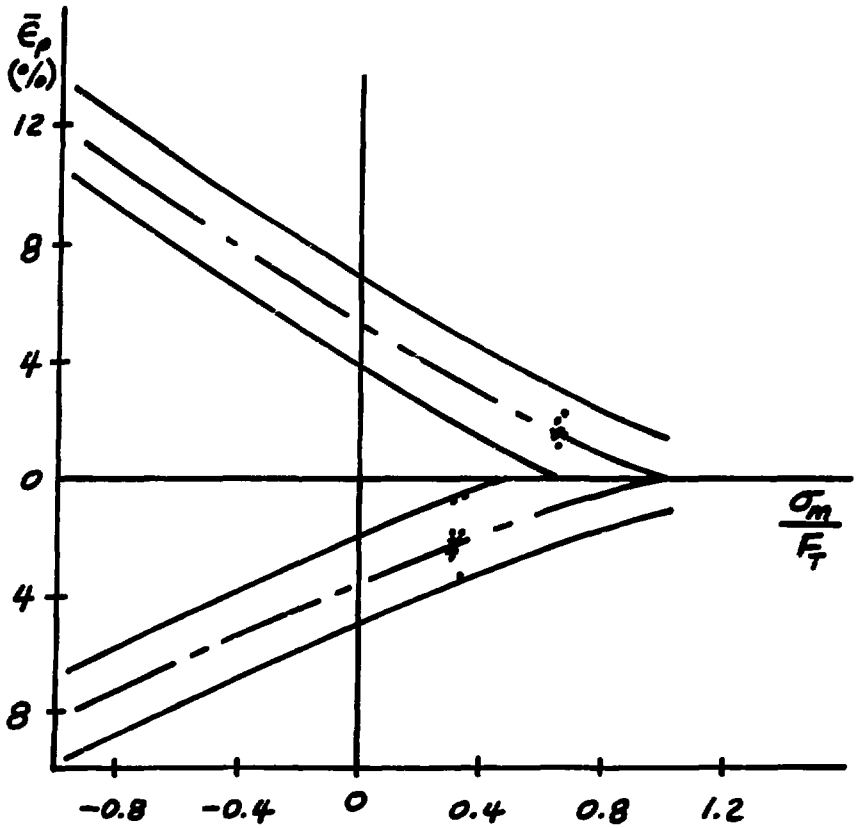

Figure 18

Transformed Stress Space Bounds, Be-Pl
Plotted vs. σ_m/F_T

7. The data for the two grades of beryllium were analyzed in a similar fashion as that described in paragraphs 1 through 6 but with the use of the exponential model given in Equation (2). A normalized function of stress and strain similar to that given by Equation (7) was used, i.e.,

$$F_e = \frac{\bar{\varepsilon}_p}{A \exp^{-k\left(\sigma_m/\bar{\sigma}\right)}} \qquad (8)$$

Computed values of A and k determined from the uniaxial tension and pure shear data are listed in Table (II). A standard deviation on the selected input data was also calculated for F_e and it is listed in this table. Figures (19 and 20) are plots of these reduced input data vs. σ_m/τ.

TABLE II

Calculated Constants for Two Grades of Be for Use in Eq. (2)

	A	k	Std. Deviation of F_e for Input Data	Number of Input Data Points
XN50C	4.480	1.299	0.2877	23
P1	4.104	1.654	0.321	17

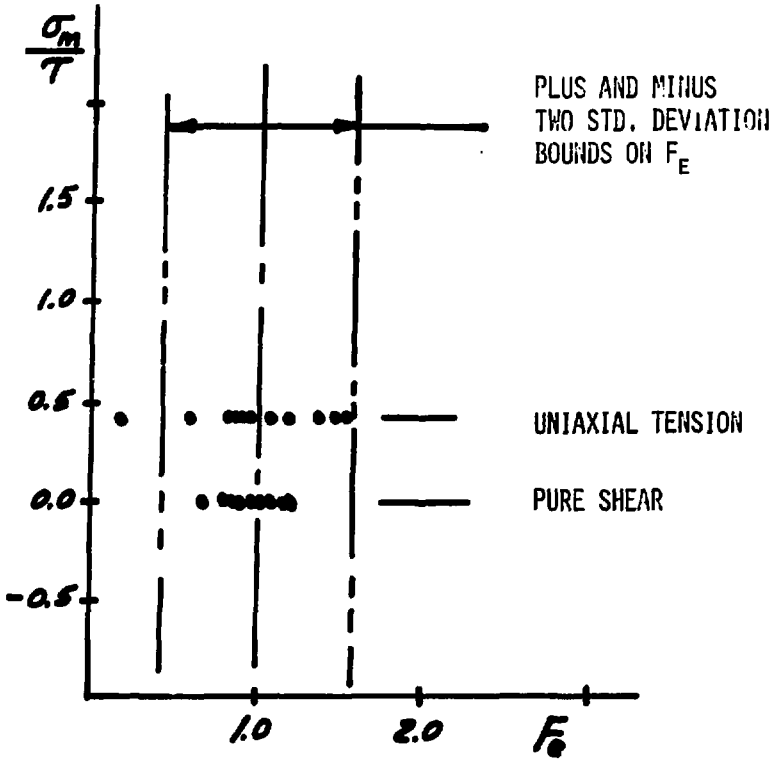

Figure 19
Plot of Reduced Values of F_e
For Be-XN50C, Input Data

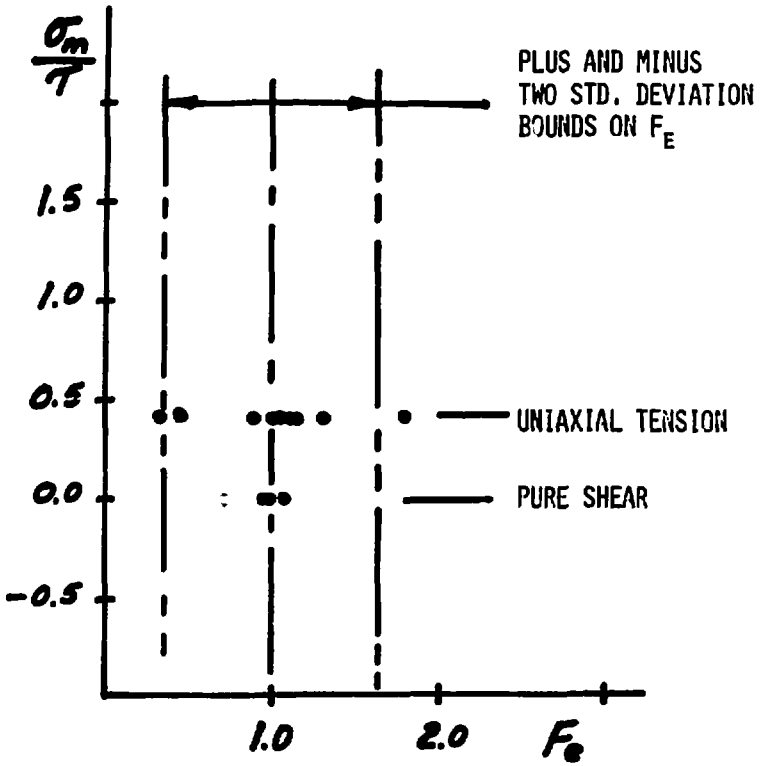

Figure 20
Plot of Reduced Values of F_e
For Be-Pl Input Data

8. Values of F_e were computed for the additional data using Equation (8) and these are plotted in Figures (21 and 22). These data are not as well contained within the expected bounds as those shown in Figures (11 and 12). In addition, the central values are shifted from unity. A histogram of the reduced Be-XN50C data is shown in Figure (23). Figure (24) is a histogram of the reduced Be-P1 data.

9. Figures (25 and 26) are plots of Equation (2) and the reduced strain data vs. σ_m/τ for the two materials.

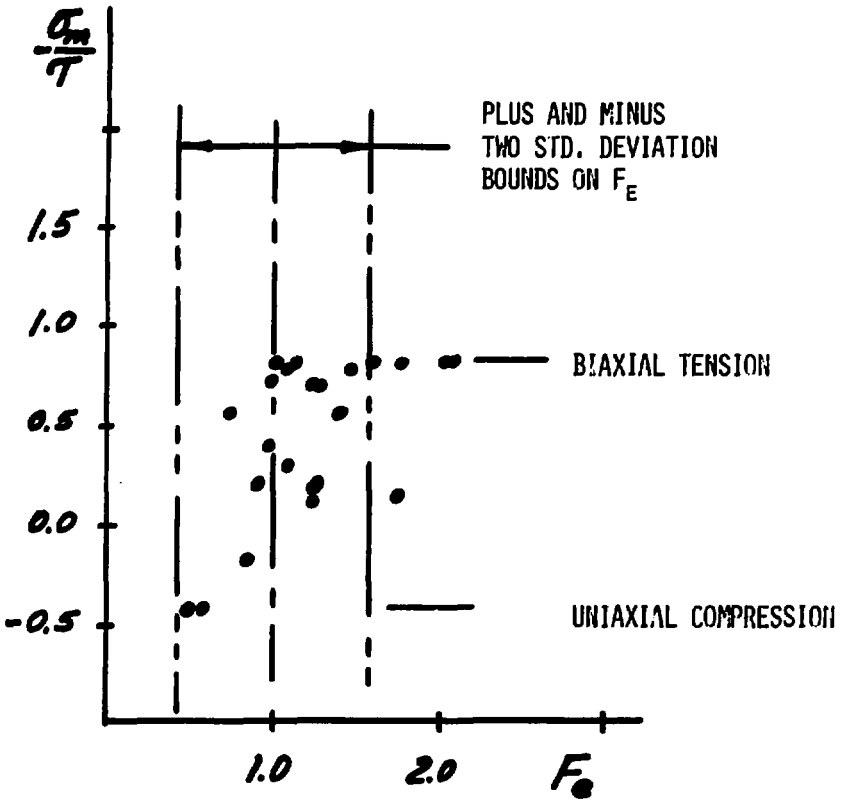

Figure 21
Plot of Reduced Values of F_e,
Be-XN50C, Remainder Data Set

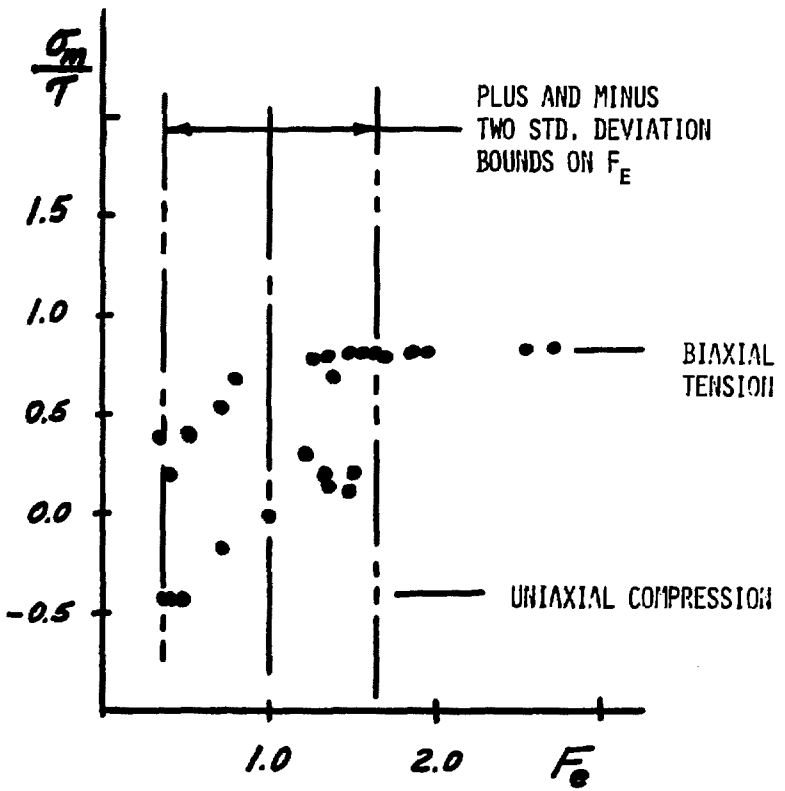

Figure 22
Plot of Reduced Values of F_e,
Be-Pl, Remainder Data Set

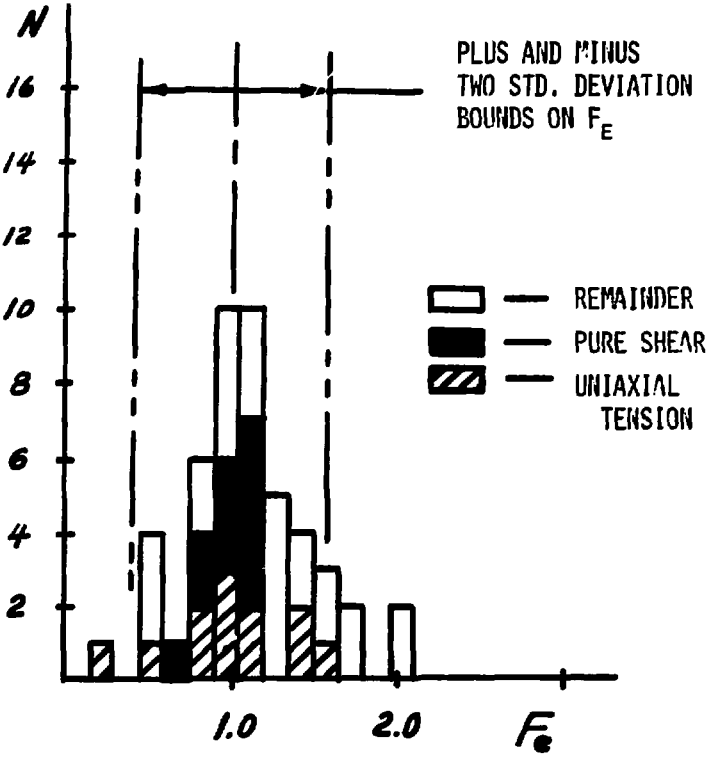

Figure 23

Histogram Plot of Reduced Be-XN50C
Data, Exponential Model

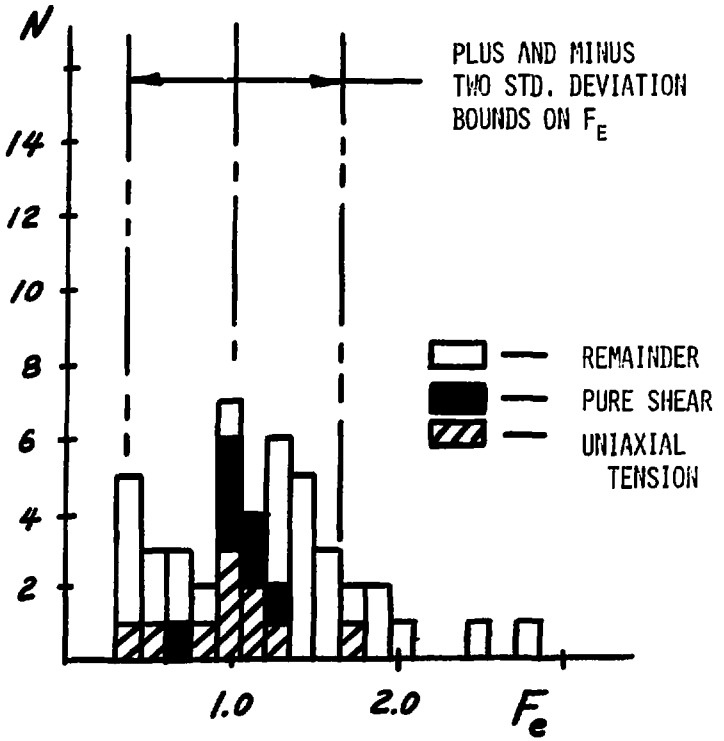

Figure 24

Histogram Plot of Reduced Be-Pl
Data, Exponential Model

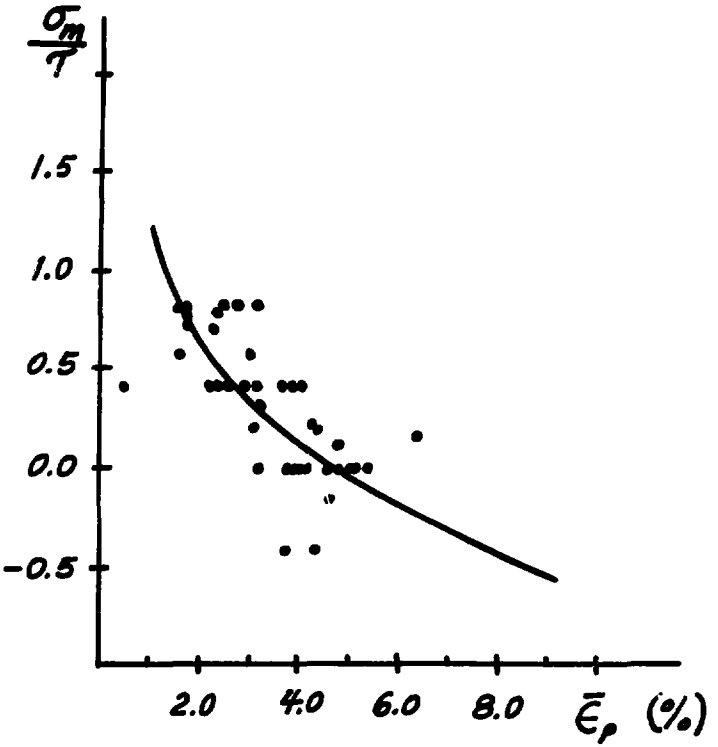

Figure 25

Plot of $\bar{\epsilon}_p$ vs. σ_m/τ for Be-XN50C Data,
Compared with Exponential Model

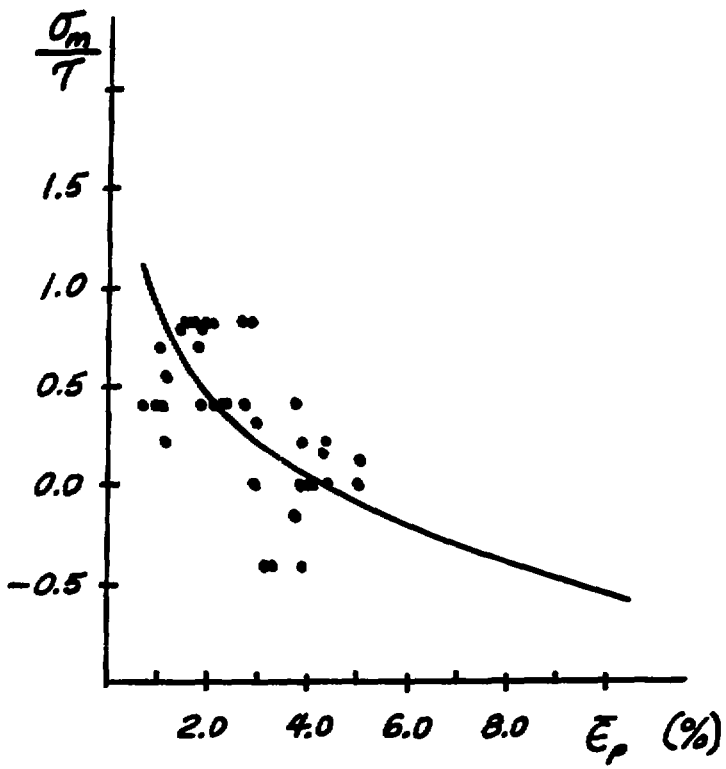

Figure 26

Plot of $\bar{\epsilon}_p$ vs. σ_m/τ for Be-Pl Data,
Compared with Exponential Model

CONCLUSIONS

1. Referenced measurements of ultimate stress and strain taken from two grades of beryllium are accurately correlated with Equation (5). This equation, used in concert with the dual characterization strength model, leads to an accurate strain at fracture prediction technique. These results generally follow the exponential mean stress model but maintain essential vector orientations of stress and strain at fracture.

2. The exponential mean stress model, Equation (2), generally follows the measured data plots but suffers from loss of stress vector orientation effects.

3. The methods used in developing Figures (17 and 18) lead to an apparently useful method of determining a lower bound (for reliable design purposes) on plastic strain at fracture.

REFERENCES

1. McClintock, F. A., "A Criterion for Ductile Fracture by Growth of Holes, "J. Appl. Mech., June 1968, pp. 363-371.

2. Rice, J. R., and Tracey, D. M., "On the Ductile Enlargement of Voids in Triaxial Stress Fields," J. Mech. Phys. Solids, June 1969, Vol. 17, No. 3, pp. 201-217.

3. Hancock, J. W., and MacKenzie, A. C., "On the Mechanisms of Ductile Failure in High-Strength Steels Subjected to Multi-Axial Stress-States," J. Mech. Phys. Solids, 1976, Vol. 24, pp. 147-169.

4. Priddy, T. G., Benzley, S. E., and Johnson, R. L., "The Dual Characteristics of Yield and Ultimate Strengths as Applied to Two Grades of Beryllium, "SAND77-0122, National Technical Information Service, Springfield, Va., February 1977.

5. Lindholm, U. S., Yeakley, L. M., Davidson, D. L., "Biaxial Strength Tests on Beryllium and Titanium Alloys," AD/A-002137, Distributed by NTIS, U. S. Dept. of Commerce, Springfield, Va., July 1974.

6. Priddy, T. G., "A Fracture Theory for Brittle Anisotropic Materials," J. of Engr. Matl's and Tech., April 1974, pp. 91-96.